The Electronic Structure of Non-Heme Iron(III)−Hydroperoxo and Iron(III)−Peroxo Model Complexes Studied by Mössbauer and Electron Paramagnetic Resonance Spectroscopies

A. Jalila Simaan,‡ Frédéric Banse,‡ Jean-Jacques Girerd,‡ Karl Wieghardt,† and Eckhard Bill*,†

Laboratoire de Chimie Inorganique, UMR CNRS 8613, Université Paris-Sud, F-91405 Orsay, France, and
Max-Planck-Institut für Strahlenchemie, D-45470 Mülheim an der Ruhr, Germany

Received June 18, 2001

Ferric peroxo complexes are currently extensively studied due to their proposed occurrence as reactive intermediates in the catalytic oxygenation reactions of cytochrome P450[1] and bleomycin.[2] Recently, several mononuclear nonheme Fe(III)−hydroperoxo[3−7] and Fe(III)−peroxo[4b−c,5b,8,9] complexes have been prepared in solution and studied by UV−visible, EPR, Resonance Raman, and Mass Spectrometry.[10] The two species displayed in Scheme 1 have been characterized in solution as purple low-spin Fe(III)−hydroperoxo (**1**) which converts upon addition of base to a blue Fe(III)−η^2-peroxo species (**2**).[4] Here, we report a detailed study of these two compounds by EPR and Mössbauer spectroscopy.

Solutions of **1** were prepared from [(trispicMeen)FeCl]Cl·2.5H_2O (trispicMeen represents the ligand *N*-methyl-*N*,*N'*,*N'*-tris(pyridylmethyl)ethane-1,2-diamine). 100-fold excess of hydrogen peroxide was added to a 1.7 mM methanolic solution of the ferrous starting complex. Compound **1** was converted to **2** by addition of 5 equiv of Et_3N. X-band EPR and Mössbauer spectra of the 47% ^{57}Fe enriched complexes **1** and **2** were recorded at cryogenic temperatures (below 50 K).

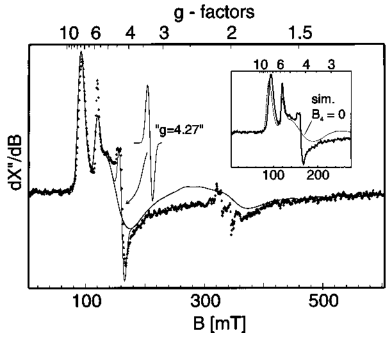

Figure 1. X-band EPR spectrum of the peroxo compound **2** (aliquot of the Mössbauer sample, 47% enriched with ^{57}Fe). Experimental conditions: temperature 10 K, microwave frequency 9.64405 GHz, modulation 1.28 mT/100 kHz. The solid line is a spin Hamiltonian simulation with parameters $D = -1.7$ cm^{-1}, $E/D = 0.08$, $\sigma(E/D) = 0.025$, $B_4 = -0.004$ cm^{-1}, $g = 2$, and Gaussian line width $\Gamma = 60$ mT (at $g = 1$, frequency dependent part only, isotropic). The arrow marks an additional Gaussian signal of a rhombic Fe(III) high-spin contamination, which was simulated with an isotropic effective g value of 4.27. The inset shows the low-field part of the experimental spectrum with alternative simulations with $B_4 = 0$ (dashed line).

Scheme 1

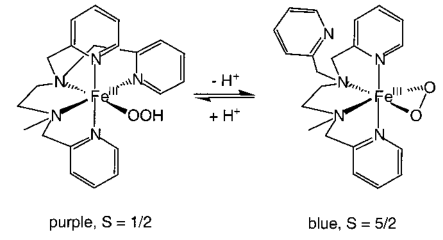

1 **2**

The EPR spectrum of **1** displays a characteristic low-spin ferric spectrum ($S = 1/2$, $g = 2.12$, 2.19, 1.95), as reported previously,[4] and an ubiquitous high-spin signal at $g = 4.3$ ($S = 5/2$ and $E/D = 1/3$). In agreement with the corresponding Mössbauer spectra, it is established that the latter signal amounts to ca. 12% of total iron in our best preparations. It is most probably due to an oxidative deterioration product of **1**.

Figure 1 shows the X-band EPR spectrum of **2** at 10 K. Prominent derivative signals at $g = 7.4$, 5.7, and 4.5 are typical for a high-spin ferric species ($S = 5/2$). In addition, an isotropic weak signal at $g = 4.27$ is observed and assigned to deterioration products. Additional very weak signals at $g = 2$ are due to the presence of residual low-spin complexes. Thus, **2** exhibits a signal of a high-spin Fe(III) ion with almost axial zero-field splitting (ZFS).[4b] The signals at $g \approx 7.4$ and $g \approx 4.5$ are assigned to the

---

* To whom correspondence should be addressed. E-mail: bill@mpi-muelheim.mpg.de.

‡ Université Paris-Sud.

† Max-Planck-Institut für Strahlenchemie.

(1) (a) Sono, M.; Roach, M. P.; Coulter, E. D.; Dawson, J. H. *Chem. Rev.* **1996**, *96*, 2841. (b) Selke, M.; Valentine, J. S. *J. Am. Chem. Soc.* **1998**, *120*, 2652. (c) Davydov, R.; MacDonald, I. D. G.; Makris, T. M.; Sligar, S. G.; Hoffman, B. M. *J. Am. Chem. Soc.* **1999**, *121*, 10654. (d) Davydov, R.; Yoshida, T.; Ikeda-Saito, M.; Hoffman, B. M. *J. Am. Chem. Soc.* **1999**, *121*, 10656.

(2) (a) Burger, R. M.; Peisach, J.; Horwitz, S. B. *J. Biol. Chem.* **1981**, *256*, 11636. (b) Sam, J. W.; Tang, X.-J.; Peisach, J. *J. Am. Chem. Soc.* **1994**, *116*, 5250. (c) Que, L., Jr.; Ho, R. Y. N. *Chem. Rev.* **1996**, *96*, 2607. (d) Solomon, E. I.; Brunold, T. C.; Davis, M. I.; Kemsley, J. N.; Lee, S. K.; Lehnert, N.; Neese, F.; Skulan, A. J.; Yang, Y.-S.; Zhou, J. *Chem. Rev.* **2000**, *100*, 235.

(3) (a) Lubben, M.; Meetsma, A.; Wilkinson, E. C.; Feringa, B.; Que, L. Jr. *Angew. Chem., Int. Ed. Engl.* **1995**, *34*, 1512. (b) Kim, C.; Chen, K.; Kim, J.; Que, L., Jr. *J. Am. Chem. Soc.* **1997**, *119*, 5964. (c) Ho, R. Y. N.; Roelfes, G.; Feringa, B. L.; Que, L., Jr. *J. Am. Chem. Soc.* **1999**, *121*, 264. (d) Roelfes, G.; Lubben, M.; Chen, K.; Ho, R. Y. N.; Meetsma, A.; Genseberger, S.; Hermant, R. M.; Hage, R.; Mandal, S. K.; Young, V. G., Jr.; Zang, Y.; Kooijman, H.; Spek, A. L.; Que, L., Jr., Feringa, B. L. *Inorg. Chem.* **1999**, *38*, 1929.

(4) (a) Mialane, P.; Novorojkine, A.; Pratviel, G.; Azéma, L.; Slany, M.; Godde, F.; Simaan, A.; Banse, F.; Kargar-Grisel, T.; Bouchoux, G.; Sainton, J.; Horner, O.; Guilhem, J.; Tchertanov, L.; Meunier, B.; Girerd, J.-J. *Inorg. Chem.* **1999**, *38*, 1085−1092. (b) Simaan, A. J.; Banse, F.; Mialane, P.; Kargar-Grisel, T.; Bouchoux, G.; Boussac, A.; Un, S.; Girerd J.-J. *Eur. J. Inorg. Chem.* **1999**, 993−996. (c) Simaan, A. J.; Döpner, S.; Banse, F.; Bourcier, S.; Bouchoux, G.; Boussac, A.; Hildebrandt, P.; Girerd, J. J. *Eur. J. Inorg. Chem.* **2000**, 1627.

(5) (a) Bernal, I.; Jensen, M.; Jensen, K. B.; MacKenzie, C. J.; Toftlund, H.; Tuchagues, J.-P. *J. Chem. Soc., Dalton Trans.* **1995**, 3667. (b) Jensen, K. B.; McKenzie, C. J.; Nielsen, L. P.; Pedersen, J. Z.; Svendsen, H. M. *Chem. Commun.* **1999**, 1313.

(6) De Vries, M. E.; La Crois, R. M.; Roelfes, G.; Kooijman, H.; Spek, A. L.; Hage, R.; Feringa, B. L. *Chem. Commun.* **1997**, 1549.

(7) Lippai, I.; Magliozzo, R. S.; Peisach, J. *J. Am. Chem. Soc.* **1999**, *121*, 780.

(8) (a) Ahmad, S.; McCallum, J. D.; Shiemke, A. K.; Appelman, E. H.; Loehr, T. M.; Sanders-Loehr, J. *Inorg. Chem.* **1988**, *27*, 2230. (b) Neese, F.; Solomon, E. I. *J. Am. Chem. Soc.* **1998**, *120*, 12829.

(9) Ho, R. Y. N.; Roelfes, G.; Hermant, R.; Hage, R.; Feringa, B. L.; Que, L. Jr. *Chem. Commun.* **1999**, 2161.

(10) Girerd, J. J.; Banse, F.; Simaan, A. J. *Structure and Bonding*; Springer-Verlag: New York, 2000; Vol. 97, pp 145−177.

10.1021/ic010635e CCC: $20.00

effective values $g'_y(1/2)$ and $g'_x(1/2)$ of the $m_s = \pm 1/2$ Kramers doublet, respectively. The signal at $g \approx 5.7$ corresponds to the effective $g'_z(3/2)$ of the middle doublet $m_s = \pm 3/2$. From the temperature dependence of the relative subspectra intensities (2−15 K), a negative axial ZFS parameter ($D < 0$) was established with $m_s = \pm 1/2$ being the excited state. We have successfully simulated the spectrum only by using the somewhat unusual spin Hamiltonian (eq 1).

$$H = D\left[S_z^{\,2} - \frac{S(S+1)}{3} + \frac{E}{D}(S_x^{\,2} - S_y^{\,2})\right] + O_4 + \mu_B \mathbf{B}\underline{\underline{\mathbf{g}}}\mathbf{S} \quad (1)$$

$$\text{with} \quad O_4 = -2/3 B_4[O_4^{\,0} + 20\sqrt{2}\,O_4^{\,3}] + B_4^{\,0}O_4^{\,0}$$

O_4 is a phenomenological symmetry adapted fourth order term in the usual effective spin Hamiltonian. The O_4^m terms represent equivalent operators of fourth degree in S and the parameters B_4 and B_4^0 parametrize cubic and trigonal contributions to the ZFS.[11] We set B_4^0 to zero and restricted the optimization to values of D, E/D, and B_4. The physical effect of the additional ZFS term is a mixing of $m_s = \pm 1/2$ and $\pm 5/2$ levels, which introduces a relative shift of the energies and effective g values of these Kramers doublets.

In agreement with the Mössbauer spectra (see below), a satisfactory fit was obtained with $D = -1.7$ cm^{-1}, $E/D = 0.08$, and $B_4 = -0.004$ cm^{-1} (see Figure 1). We note that it has not been possible to reproduce the EPR spectrum without the fourth-order term in eq 1. Indeed, neither the exact position of the different resonances nor their relative intensities could be satisfactorily fitted without this term. With the best value $B_4 = -0.004$ cm^{-1}, the simulated derivative lines appear at effective g values $g'_y(1/2) = 7.43$, $g'_x(1/2) = 4.53$, and $g'_z(3/2) = 5.69$, in contrast to $g'_y(1/2) = 7.74$, $g'_x(1/2) = 4.22$, and $g'_z(3/2) = 5.62$ for $B_4 = 0$. The variation shows the influence of B_4 on the $m_s = \pm 1/2$ wavefunctions. A simulation for the latter case is shown in the inset of Figure 1. Moreover, the peculiar differences in line widths of the resonances, particularly $g'_y(1/2)$ and $g'_x(1/2)$, could be easily simulated by introducing an E/D strain. A Gaussian distribution for the rhombicity parameter was adopted, whereas the intrinsic linewidth was taken to be frequency constant, which leads to a variation of the linewidths in the field swept spectrum according to the respective g values. Using this model the experimental pattern is nicely reproduced with a half width for the E/D distribution of $\sigma(E/D) = 0.025$.

Magnetic Mössbauer spectra of the Fe(III)OOH and Fe(III)O$_2$ species **1** and **2** were measured at liquid helium temperature with applied fields of 0.04, 3, and 7 T. As shown in Figure 2, the spectra of the hydroperoxo complex **1** are rather broad and show only weak overall splitting. This is quite typical for Fe(III) low-spin systems.[12] The pattern is superimposed by the widely split six-line spectrum of a minor high-spin ferric component (ca. 12%), which was simulated adopting a rhombic $S = 5/2$ species using the EPR parameters from above. The pronounced asymmetry of the low-spin spectra of **1** indicates an anisotropy of the hyperfine tensor in conjunction with a large quadrupole splitting. The small isomer shift, δ, of 0.19 mm s^{-1} at 4.2 K is typical for an iron(III) low-spin complex.[12] The spectra were simulated with the usual spin Hamiltonian approach for $S = 1/2$ by using a magnetic hyperfine coupling tensor $\underline{\underline{\mathbf{A}}}/g_N\beta_N = (+7.77, -3.65, -41.09)$ T, and the anisotropic g values were determined by EPR. The elements of the g matrix were all set to be positive. This is not a constraint since the Mössbauer spectra are sensitive only for the products g_iA_i. The electric field gradient (efg) tensor has a large, negative main component, $V_{zz} = -2.01$ mm s^{-1}, and a relatively small asymmetry parameter, $\eta = 0.4$. The fits could be slightly improved by the introduction of an Euler rotation of the efg tensor around the z axis by an angle $\alpha = 43°$ with respect the principal axes systems of $\underline{\underline{\mathbf{A}}}$ and $\underline{\underline{\mathbf{g}}}$ tensors; rotations around the x or y axes were found to be less than 2°, which indicates colinearity of the principal z axes of the three coupling tensor tensors.

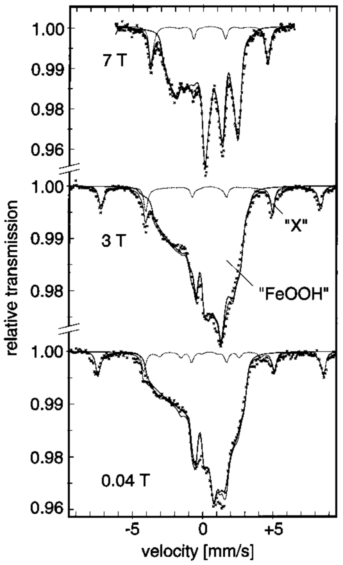

Figure 2. Magnetic Mössbauer spectra of complex **1** measured at 4.2 K with fields of 0.04, 3, and 7 T applied perpendicular to the γ rays. The solid line is a simulation for the hydroperoxo species "FeOOH" with parameters $S = 1/2$, $\mathbf{g} = (2.12, 2.19, 1.95)$, $\delta = 0.19$ mm s^{-1}, $\Delta E_Q = -2.01$ mm.s^{-1}, $\eta = 0.4$, $\alpha = 43°$ (Euler angle), and $\underline{\underline{\mathbf{A}}}/g_N\beta_N = (7.77, -3.65, -41.09)$ T. The dashed line represents a rhombic Fe(III) high-spin contamination "*X*" ($S = 5/2$, $D = 1.5$ cm^{-1}, $E/D = 0.33$, $g = 2$, $\underline{\underline{\mathbf{A}}}/g_N\beta_N = -21$ T, 12% relative intensity).

The Mössbauer parameters can be qualitatively rationalized in a ligand field description, which strongly implies a low-spin Fe(III) complex with $(d_{xz}, d_{yz})^4(d_{xy})^1$ electron configuration, in excellent agreement with the previous interpretation of the EPR g values of this complex[4c] and other models[10] of activated Bleomycin.[13] The parametrization uses the crystal-field model developed by Griffith[14] for the description of the spin−orbit interaction of distorted $(t_{2g})^5$ complexes. The best solutions for **1** within Taylor's "proper axes" system ($V < 2/3\ \Delta$)[15] imposes a relatively large axial splitting to the t_{2g} orbital set, $\Delta/\lambda = -11.4$ with a weak rhombic distortion, $V/\lambda = 4$.[4c,10] This splitting scheme was interpreted as the result of dominating antibonding interaction of the iron $|xy\rangle$ orbital with the π^* orbital of the hydroperoxo group (if this is positioned along the y direction).[10,13] The resulting anisotropy of the valence electrons caused by the electron *hole* in a single "pan-cake" shaped d_{xy} orbital is expected to induce a strong *negative* valence contribution to the main component of the efg in the z direction (and a small asymmetry parameter), in accordance with the experimental observation. The asymmetry of the experimental magnetic hyperfine tensor $\underline{\underline{\mathbf{A}}}$ is also consistent with the d_{xy} hole picture. The orbital coefficients in this model[16] lead to strong orbital and spin-dipolar contributions to $\underline{\underline{\mathbf{A}}}$, which explain the large, negative A value in the direction of the efg main component. The best solution for the $\underline{\underline{\mathbf{A}}}$ tensor that can be obtained in the ligand-field picture (with $\kappa = 0.35$, P

---

(11) Abragam, A.; Bleaney, B. *Electron Paramagnetic Resonance of Transition Ions*; Oxford University Press: Oxford, 1970.

(12) Debrunner, P. G. *Mössbauer Spectroscopy of Iron Porphyrins*; Debrunner, P. G., Ed.; VCH: Weinheim, 1989; Vol. III, pp 137−234.

(13) Veselov, A.; Sun, H.; Sienkiewicz, A.; Taylor, H.; Burger, R. M.; Scholes, C. P. *J. Am. Chem. Soc.* **1995**, *117*, 7508−7512.

(14) Griffith, J. S. *Proc. R. Soc. London, A* **1956**, *235*, 23−36.

(15) Taylor, C. P. S. *Biochim. Biophys. Acta* **1977**, *491*, 137−149.

(16) Oosterhuis, W. T.; Lang, G. *Phys. Rev.* **1969**, *178*, 439−456.

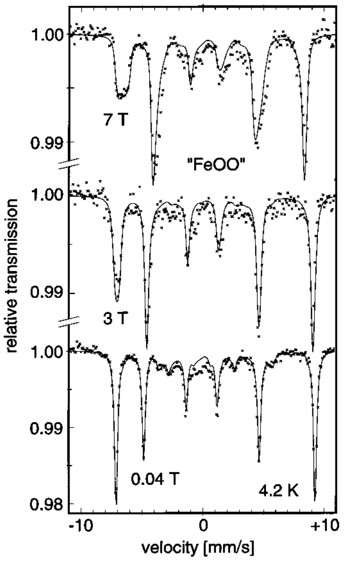

Figure 3. Magnetic Mössbauer spectra of complex **2** measured at 4.2 with fields of 0.04, 3, and 7 T applied perpendicular to the γ rays. The solid line is a simulation for the peroxo species "FeOO" with parameters $S = 5/2$, $D = -1.7$ cm^{-1}, $E/D = 0.08$, $B_4 = -0.004$ cm^{-1}, $g = 2$, $\delta = 0.64$ mm s^{-1}, $\Delta E_Q = +1.37$ mm.s^{-1}, $\eta = 0.98$, and $\underline{\underline{A}}/g_N\beta_N = (-22.71, -22.09, -20.40)$ T.

= 49.25 T) is $\underline{\underline{A}}/g_N\beta_N = (+2.3, -6.0, -41.1)$ T, which is very close to the experimental value. Hence, the magnetic Mössbauer spectra support the description of **1** as a system with $(d_{xz}, d_{yz})^4$-$(d_{xy})^1$ electron configuration with a destabilized d_{xy} orbital in the t_{2g} orbital set, which is due to π interaction of with the OOH group. We note that the Griffith model might not be fully valid in its simplest form as it was applied here if the symmetry is less than rhombic. Recently, such a deviation was noted for another low-spin Fe(III) center from a rotation of the $\underline{\mathbf{g}}$ and $\underline{\underline{A}}$ tensors, as determined from complementary ^{57}Fe EPR and Mössbauer data.[17] We cannot exclude that such low-symmetry effects are also prevailing in the electronic structure of **1**, which is entirely asymmetric. (We gratefully acknowledge a reviewer's comment pointing out this limitation.)

The peroxo complex **2** exhibits a well resolved magnetic hyperfine pattern in the applied-field Mössbauer spectra, as shown in Figure 3. The large overall splitting indicates the presence of strong internal fields on the order of 54 T, which is typical for high-spin ferric ions.[18] The spectra were readily simulated by using the ZFS parameters derived from the EPR simulations. They corroborate particularly the negative sign of the axial ZFS parameter. We mention that a very similar fit could be obtained without the fourth order parameter B_4, yielding slightly different axial and rhombic parameters, $D = -1.1$ cm^{-1} and $E/D = 0.08$. For consistency, however, the same model parameters were applied as used in the EPR simulations. The other Mössbauer parameters obtained are: i) the large isomer shift $\delta = 0.64$ mm s^{-1}, ii) the large quadrupole splitting $\Delta E_Q = +1.37$ mm s^{-1} with maximal asymmetry $\eta = 0.98$, and iii) the slightly anisotropic magnetic hyperfine tensor $\underline{\underline{A}}/g_N\beta_N = (-22.71, -22.09, -20.40)$ T. The isomer shift and quadrupole splitting of compound **2** are both unusually large for typical high-spin ferric complexes,[18] but interestingly, they closely resemble those of the peroxo−diferric intermediate of methane monooxygenase[19] and those of a synthetic (μ-1,2-peroxo)diiiron(III) compound ($\delta = 0.66$ mm s^{-1}, $\Delta E_Q = 1.40$ mm s^{-1}).[20] A previous Mössbauer and EPR investigation of a peroxoferriporphyrin complex[21] also revealed similar properties for the FeOO unit in a heme environment. Particularly, the isomer shift and magnetic hyperfine coupling constants are large and very close to those of **2**, whereas the quadrupole splitting is significantly lower (+0.62 mm s^{-1}). It is interesting to note that similarly high values of δ are otherwise observed only for the Fe(III) high-spin site of nitrosylated nonheme compounds with $\{FeNO\}^7$ centers.[22,23] The large isotropic part of the magnetic hyperfine tensor ($\underline{\underline{A}}/g_N\beta_N = -21.7$ T) is also in the upper range of typical values found for ionic ferric systems (−20 to −22 T).[24] Thus, the Mössbauer parameters reveal the presence of a high-spin Fe(III) moiety with relatively low total covalent delocalization of valence electrons. The unusally large quadrupole splitting for a 3d $(t_{2g})^3(e_g)^2$ configuration resembles those of μ-oxo-diiron(III) complexes. The origin of those values was assigned to prevailing *anisotropy* of the 3d population due to anisotropic covalency, as it is induced by a single short oxo bond.[25] MO calculations on $[Fe(EDTA)(O_2)]^{-3}$ support the spectroscopically deduced side-on binding mode of the peroxo ligand.[8b] From this model study, a dominating strong, covalent σ bond between Fe d_{xy} and peroxide π was identified, which provides a perfect explanation for the large efg and the anisotropy of the $\underline{\underline{A}}$ tensor for the peroxo complex **2**.

Supporting Information Available: Experimental Section. This material is available free of charge via the Internet at http://pubs.acs.org.

IC010635E

---

(17) Popescu, V. C.; Münck, E.; Fox, B. G.; Sanakis, Y.; Cummings, J. R.; Turner, I. M.; Nelson, M. J. *Biochemistry* **2001**, *40*, 7984−7991.

(18) Greenwood, N. N.; Gibb, T. C. *Mössbauer Spectroscopy*; Chapman and Hall Ltd.: London, 1971.

(19) (a) Liu, K. E.; Valentine, A. M.; Wang, D.; Huynh, G. H.; Edmonson, D. E.; Salifoglou, A.; Lippard, S. J. *J. Am. Chem. Soc.* **1995**, *117*, 10174. (b) Liu, K. E.; Valentine, A. M.; Qiu, D.; Edmonson, D. E.; Appelman, E. H.; Spiro, T. G.; Lippard, S. J. *J. Am. Chem. Soc.* **1995**, *117*, 4997.

(20) Kim, K.; Lippard, S. J. *J. Am. Chem. Soc.* **1996**, *118*, 4914.

(21) Burstyn, J. N.; Roe, J. A.; Miksztal, A. R.; Shaevitz, B. A.; Lang, G.; Valentine, J. S. *J. Am. Chem. Soc.* **1988**, *110*, 1382−1388.

(22) Rodriguez, J. H.; Xia, Y.-M.; Debrunner, P. G. *J. Am. Chem. Soc.* **1999**, *121*, 7846−7863.

(23) Hauser, C.; Glaser, T.; Bill, E.; Weyhermüller, T.; Wieghardt, K. *J. Am. Chem. Soc.* **2000**, *122*, 4352−4365.

(24) Srivastava, J. K.; Bhargara, S. C.; Iyengar, P. K.; Thosar, B. V. In *Advances in Mössbauer Spectroscopy*; Thosar, B. V., Iyengar, P. K., Eds.; Elsevier: New York, 1983; pp 1−121.

(25) Rodriguez, J. H.; Xia, Y.-M.; Debrunner, P. G.; Chaudhuri, P.; Wieghardt, K. *J. Am. Chem. Soc.* **1996**, *118*, 7542−7550.